

Burning and reading ensembles of spectral holes by optical frequency combs: Demonstration in rare-earth-doped solids and application to laser frequency stabilization

René Oswald , Alexander Yu. Nevsky , and Stephan Schiller **Institut für Experimentalphysik, Heinrich-Heine-Universität Düsseldorf, 40225 Düsseldorf, Germany* (Received 8 June 2021; accepted 19 November 2021; published 13 December 2021)

We describe a spectroscopic method applicable to inhomogeneously broadened transitions. As a test system we use suitable rare-earth-doped solids in which persistent spectral holes can be burned on weakly allowed electronic transitions. These systems are of interest as frequency references for the stabilization of laser frequencies. In all experiments so far, spectral holes are burned and read out individually. Here we present a demonstration of simultaneous burning and readout of sets of spectral holes, containing up to 1024 individual spectral holes, by a comb of laser frequencies. The simultaneous readout of such a set leads to an effective compound signal that has a higher signal-to-noise ratio. Here, an improvement by a factor of 20 was obtained for a set of 512 spectral holes. We use the method to stabilize the frequency of a laser and characterize its stability.

DOI: [10.1103/PhysRevA.104.063111](https://doi.org/10.1103/PhysRevA.104.063111)

I. INTRODUCTION

The impressive progress in the development of optical clocks [1–5] has to a large extent become possible thanks to significant improvements of the frequency stability of the lasers used to interrogate the ultranarrow transitions in cold atoms. Linewidth narrowing of these “clock” lasers is typically achieved by active stabilization of their frequency to a resonance of an ultrastable high-finesse optical cavity. In such an implementation, fractional laser frequency instability as low as 4×10^{-17} at 1-s averaging time has been achieved [1,6,7]. However, the fundamental limitation for further reducing the laser frequency instability is associated with thermal-noise induced fluctuations of the optical path length in the reference cavities [8,9]. One promising alternative to optical cavities is ultranarrow absorption lines obtained by persistent spectral hole (SH) burning in rare-ion-doped solids at cryogenic temperatures [10]. This approach has been considered for frequency stabilization of lasers for more than two decades [10–14]. In recent years, the performance of this technique has progressed substantially but has not yet approached that of state-of-the-art cavity-based frequency stabilization [15–19].

A spectral hole reference differs from other references in that its spectral shape is modified in time. First, it is modified by the probe laser radiation itself, that produces further hole burning [20]. Second, on a long time scale, SHs undergo spectral diffusion [21,22]. These modifications of spectral shape and spectral position impose limitations on the achievable frequency stability of the stabilized laser, and should be minimized. Since the burning effect increases with laser power, it is desirable to reduce the laser power during interrogation. However, a reduction of the laser power reduces the signal-to-noise (S/N) ratio in detection and, as a result,

degrades the frequency stability. To overcome this problem, the use of multiple SHs (a SH ensemble) was proposed for laser frequency stabilization and a fractional frequency instability at the level of $10^{-15}/\sqrt{\tau}$ (τ is the averaging time) was demonstrated [16,17]. In these studies, a SH ensemble was first prepared by sequential burning. Then, laser frequency stabilization occurred to a single SH from this ensemble during a short time interval. Another SH was then randomly selected, the laser stabilized on it, and so forth. Because of the short interaction time with a particular SH, a relatively high laser interrogation power was allowable, that did not significantly modify the SH. This “hole hopping” procedure could continue for a long time, depending only on the number of available SHs. Another approach for reducing the influence of the laser power on the frequency stabilization to SHs is based on a heterodyne detection. This allowed achieving a fractional laser frequency instability in the low 10^{-14} range for integration times between 1 and 100 s [18]. Using a double-heterodyne detection scheme, Galland *et al.* recently demonstrated frequency instability of 1.7×10^{-15} at 1 s [19].

In the approach described in this paper, a monochromatic laser wave is converted into a frequency comb, a superposition of a large number of spectral components, all of similar power. This comb, having appropriately high total power, simultaneously burns an ensemble of SHs. Subsequently, the complete SH ensemble can be simultaneously read out by the same laser comb (see Fig. 1).

Considering a typical inhomogeneous spectral width of several GHz for the 580-nm absorption line in $\text{Eu}^{3+} : \text{Y}_2\text{SiO}_5$ crystals at cryogenic temperatures, and a typical SH linewidth of several kHz, we recognize the potential of burning 10^5 individual SHs in the crystal. An appropriate frequency comb could then probe this large ensemble in parallel. A strongly improved S/N ratio may result, attractive for frequency stabilization purposes, especially on short integration time scales (seconds).

*step.schiller@hhu.de

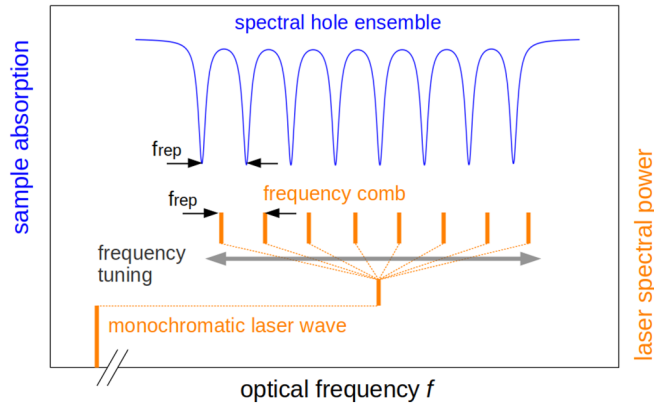


FIG. 1. Principle of the technique implemented in this paper. An ensemble of spectral holes (blue), regularly spaced in frequency space, is interrogated by a frequency comb (orange). In our setup, this comb is generated from a monochromatic laser wave (orange) by a modulator. The frequency offset f_{rep} between adjacent comb components is chosen to be identical to that of the spectral holes. In order to perform spectroscopy, the comb as a whole is tuned in frequency (gray double arrow).

In the application to frequency stabilization, the readout laser power is appropriately reduced, in order to obtain a suitably low power in each spectral component. This minimizes the influence of additional hole burning on the laser stabilization process. However, the total laser power detected, arising from all comb components, can be high enough to achieve a good S/N ratio. Compared to the work in Ref. [16], the present approach allows the laser to be continuously locked to SHs without the need for frequency hopping and relocks.

II. FREQUENCY-COMB SPECTRUM GENERATION

A monochromatic light wave can be transformed into an ensemble of spectral components regularly spaced in frequency by sending it through an electro-optic (EOM) or acousto-optic (AOM) light modulator driven by an appropriately time-dependent voltage. We consider here spectral ensembles where the relative phase between the components are well defined, i.e., constant in time. These ensembles can be called “frequency combs.” It is well known that with one EOM or a pair of EOMs driven by a sinusoidal electric signal, both phase and amplitude modulation can be implemented. A spectrum of evenly spaced components results, but the number of spectral components (on the order of 20) is limited by the achievable modulation index and a flat spectrum is difficult to realize [23,24]. Recently, a wide and flat optical spectrum containing 1500 components has been demonstrated using AOMs in an optical loop configuration [25]. This approach requires an efficient optical amplifier, but such a device is not always available for a given laser wavelength of interest. A frequency comb, however, can also be easily obtained by modulating the amplitude of the rf signal driving a single AOM. We shall discuss this in the following.

A. Short-pulse modulation

Consider a simple case: the rf signal to an AOM, having a typical frequency on the order of 100 MHz, is modulated in amplitude by a regular and infinitely long train of short rectangular pulses varying between zero and unity. The spectrum of the laser wave diffracted and frequency shifted by the AOM has a sinc-shaped envelope with an underlying comb structure. The quantitative aspects of the spectrum are determined by the modulation parameters: the overall spectral width is inversely proportional to the pulse duration and the spectral separation between the components of the comb is equal to the pulse repetition rate. For a fast AOM with an output wave rise time on the order of several 10 ns and a modulation bandwidth of several MHz, a spectrum having several MHz bandwidth and component separation of, e.g., 10 kHz, is achievable, resulting in a few hundred spectral components in total. Since the envelope of the spectrum has a sinc-function shape the spectral components vary substantially in amplitude.

For application to SH burning, we must consider that the burning process depends on the power of the spectral component. Thus, if radiation with the above spectrum is used to burn an ensemble of spectral holes, the holes will have a varying depth. Another drawback of short-pulse modulation is the small average rf power applied to the AOM compared to the peak power (which must remain below the safe threshold). This leads to a strongly reduced average laser power in the diffracted beam. Thus, the power available at the laser source is not efficiently transferred to the frequency comb radiation sent to the sample.

B. Schroeder modulation

Consider now the AOM being driven by a rf voltage $V(t)$ consisting of a comb of $2N$ rf frequencies (components):

$$V(t) = \cos(2\pi f_0 t) \sum_{n=1}^N V_n \cos(2\pi n f_{\text{rep}} t + \phi_n). \quad (1)$$

The spectral components of the comb $V(t)$ have amplitudes $\frac{1}{2}V_n$ and span the frequency range $f_0 - Nf_{\text{rep}}$ to $f_0 + Nf_{\text{rep}}$ (excluding f_0), where the carrier base frequency f_0 is of the order 100 MHz and f_{rep} is of the order 10 kHz. ϕ_n denotes the individual phase of a pair of spectral components. A monochromatic wave f_L diffracted by the AOM in order +1 will then contain an optical frequency comb, comprising the $2N$ frequencies $f_L + f_0 - Nf_{\text{rep}}$ to $f_L + f_0 + Nf_{\text{rep}}$, excluding $f_L + f_0$, with phase-stable optical spectral components. If $V_n = \text{const}$, the spectrum is flat. In practice, however, the flatness is limited by the finite modulation bandwidth of the AOM. The nominal flatness is independent of the value of the phases ϕ_n , but their values determine the character of the time structure of $V(t)$ and therefore of the time-varying amplitude of the optical wave diffracted by the AOM.

As a simple example, in Fig. 2 a hypothetical rf frequency comb $V(t)$ having $N = 32$ components and $f_0 = 0$ has been plotted in the time domain for two different phase functions. The simplest case where all components have a constant phase $\phi_n = 0$ is shown in red. The time trace of this signal exhibits sharp pulses occurring at time intervals of $1/f_{\text{rep}}$ and is similar

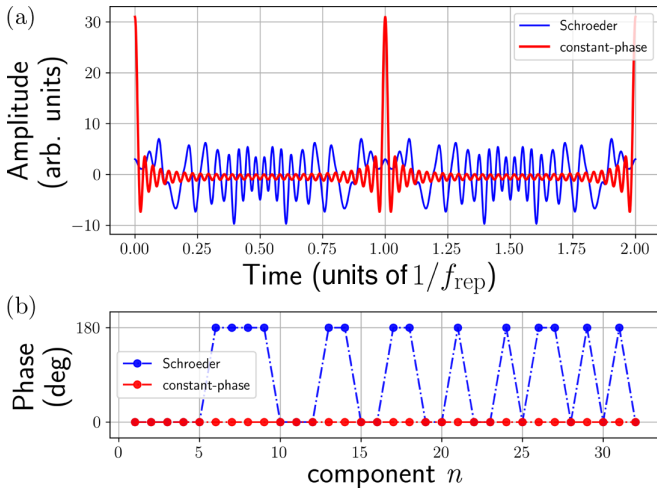


FIG. 2. Two examples of frequency combs containing 32 spectral components having equal amplitudes, but different relative phases. (a) Time traces $V(t)$ of a constant-phase-type comb (red) and a Schroeder-type comb (blue), both having zero base frequency. (b) Phases of the individual frequency components of a constant-phase-type comb with $\phi_n = 0$ (red) and Schroeder-type comb with the phases ϕ_n calculated using Eq. (2) (blue).

to the familiar femtosecond frequency comb used in optical metrology.

In contrast, in the field of telecommunications, phase functions have been derived that minimize the peak-to-peak amplitudes, i.e., the value $\Delta V_{pp} = \max[V(t)] - \min[V(t)]$. Schroeder [26] showed theoretically that if the phases ϕ_n are given by the relationship

$$\phi_{n,\text{Schroeder}} = \pi \text{round}\left(\frac{n^2}{2N}\right) \quad (2)$$

then a significantly smaller relative peak factor can be achieved than in the constant-phase case. “Relative peak factor” is defined, according to Schroeder, as ΔV_{pp} divided by $2\sqrt{2}$ times the signal’s r.m.s. value. The so-defined relative peak factor is 1 for pure sine waves. The Schroeder comb shown in the figure has a relative peak factor of 1.3, while the value is 3.5 for the constant-phase comb. The advantage of using a Schroeder-type signal is that for an amplifier that has to process the signal, and exhibits a given peak-to-peak amplitude range, a larger power gain is possible. Note how the time signal of a Schroeder frequency comb (blue) looks like a chirp with increasing frequency towards the middle of the period $1/f_{\text{rep}}$ and decreasing frequency towards the end of the period.

It is apparent that the time signal of the constant-phase frequency comb has substantial amplitude for a smaller fraction of the time than for the Schroeder frequency comb. Returning to the optical comb generated using $V(t)$, this means that for constant-phase modulation, the laser wave is reaching the sample with substantial power for a smaller fraction of the time. Given the fact that the peak power that can be made available by the overall optical system is limited, a Schroeder comb permits a larger average laser power to reach the sample. Furthermore, the constant-phase comb leads to optical pulses. These produce electrical pulses in the output of the

photodetector downstream of the sample. Filtering out these pulses adds a certain complexity to the signal processing.

C. Experimental implementation

Our experimental setup for generation of the frequency comb and for SH spectroscopy is an extension of our previous apparatus described in Ref. [27]. It is shown simplified in Fig. 3.

The apparatus contains as spectroscopy source a Littrow-configuration diode laser at 1160 nm, frequency-doubled to 580 nm in a second-harmonic generation unit. This wave has the optical frequency f_L . The radiation is frequency stabilized to an ultrastable, high-finesse ultra-low-expansion (ULE) optical cavity. The linewidth of the stabilized laser is approximately 10 Hz; its long-term frequency drift rate is approximately 0.03 Hz/s. The radiation traverses AOM2 (orange) for the generation of an optical frequency comb.

Inside the bottom left dashed box we show the components that produce, together with the AOM2, the optical frequency comb. As a first example, a comb consisting of $2N = 512$ components separated by $f_{\text{rep}} = 20$ kHz is generated. We use a 16-bit arbitrary waveform generator (AWG), programmed with the function $\sum_{n=1}^N \cos(2\pi n f_{\text{rep}} t + \phi_{n,\text{Schroeder}})$, the second factor in Eq. (1). The AWG output signal is mixed in a rf double-balanced mixer (DBM) with the rf carrier signal f_0 delivered by a DDS generator DDS1. We choose $f_0 = 200$ MHz, so as to be close to the center frequency of our AOM. The DBM provides a dual-side-band modulation producing a flat spectrum as described by Eq. (1) extending from $f_0 - N f_{\text{rep}}$ to $f_0 + N f_{\text{rep}}$ and having $2N = 512$ components in total. The carrier f_0 is not completely suppressed. The resulting rf spectrum f_{comb} is measured by the spectrum analyzer indicated in Fig. 3. The data recorded by the spectrum analyzer are reported in Fig. 4 (top). We notice a fairly good flatness with deviations of less than 1% for the individual components.

We characterized the optical comb by producing an optical heterodyne beat between the optical comb and the monochromatic input laser wave f_L . It is detected by photodetector PD B in Fig. 3 and is analyzed by the same rf spectrum analyzer. Figure 4 (bottom) presents the spectrum. The upper half of the spectrum, from 200 to 205 MHz, is flat; the lower half shows a falling slope towards 195 MHz. This is due to a decreasing AOM diffraction efficiency and a reduction in the optical efficiency in coupling to a fiber downstream of the AOM. Overall, the standard deviation of the amplitudes is 3%.

III. SPECTROSCOPY OF SPECTRAL HOLES WITH FREQUENCY COMBS

A. Setup

We carried out spectral hole burning spectroscopy on the ${}^7F_0 \rightarrow {}^5D_0$ transition of Eu^{3+} ions on the crystallographic site 1 ($\lambda = 580.03$ nm) of $\text{Eu}^{3+} : \text{Y}_2\text{SiO}_5$ in the temperature range 4.0–6.7 K. The components used for the spectroscopy are shown in Fig. 3. We use a crystal with 1.0%-rare-earth-ion concentration manufactured by Scientific Materials Corp. It is located within a permanent ring shaped magnet of approximately 0.8-T field strength along the crystal c axis and inside a closed-cycle pulse-tube-cooler (PTC) cryostat. The 580-nm

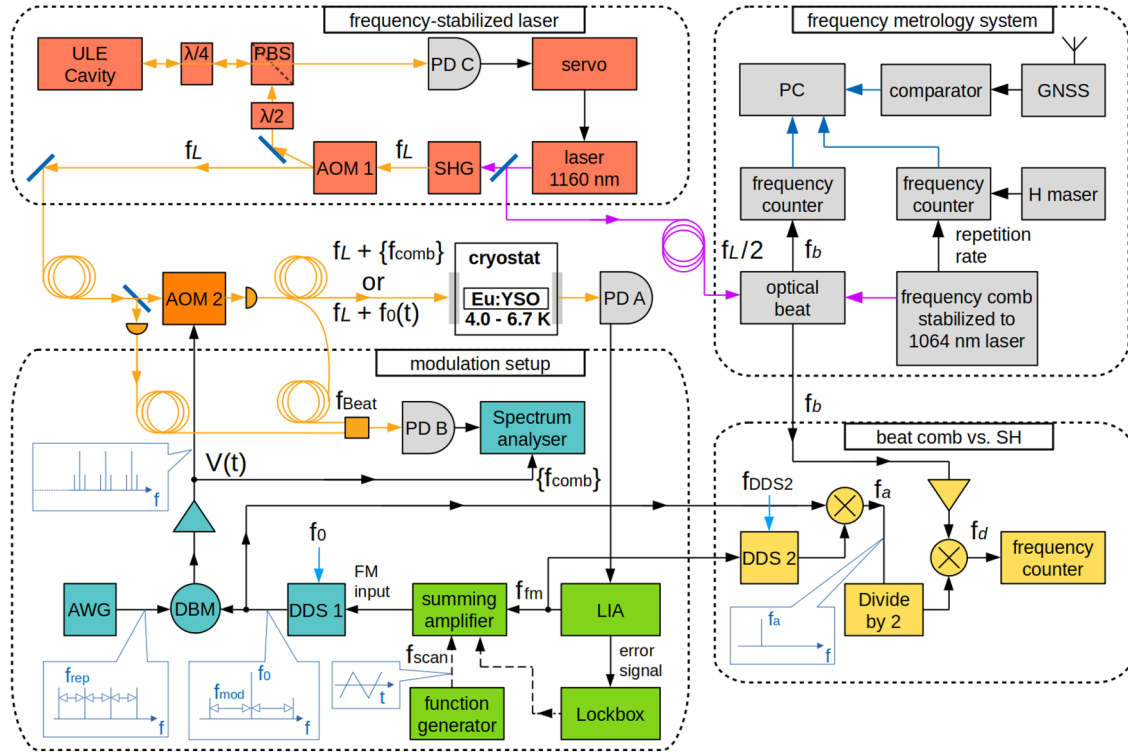


FIG. 3. Setup for frequency-comb spectroscopy of spectral holes. PD, photodetector; AOM, acousto-optic modulator; AWG, arbitrary waveform generator; LIA, lock-in amplifier; DDS, direct digital synthesis generator; DBM, double-balanced mixer; SHG, second-harmonic generator; ULE, ultra-low-expansion glass; PBS, polarizing beam splitter; GNSS, global navigation satellite system. Pink arrows and fibers: Optical fiber carrying 1160-nm radiation. Orange arrows and fibers carry 580-nm radiation. Black arrows: rf or DC signals. Blue arrows: Digital signals.

laser radiation is led into the cryostat using an optical fiber and is focused into the crystal to approximately 3-mm diameter using a fiber collimator. The D_1 and D_2 axes of the crystal are parallel to the edges of its 5×5.5 mm end faces. The laser light is linearly polarized parallel to the D_2 axis of the crystal. After passing through the crystal the light exits the cryostat through a glass window and is detected by the low-noise photodetector PD A.

B. Burning of an ensemble of spectral holes

Using the optical Schroeder comb consisting of 256 spectral components spaced by 20 kHz with a total optical power of about $1 \mu\text{W}$, we simultaneously burned an ensemble of spectral holes for 10 min. After the burning process, the AWG was turned off and spectroscopy was done by scanning the entire spectral range spanned by the SHs with a single-frequency laser wave. In practice, the function generator shown in green in Fig. 3 delivered a modulation signal with a frequency of 10 Hz and triangular shape. The signal delivered to AOM2 via the DBM was only the partially suppressed carrier f_0 with slowly swept frequency. The resulting spectral hole pattern detected by PD A is depicted in Fig. 5. It exhibits a set of 256 spectral holes with a spacing of 20 kHz, as expected. There is one additional SH, burnt by the incompletely suppressed carrier. We shall not take this into account further. The spectral width of the individual SHs is approximately 5 kHz. The slope in the signal baseline results from a variation of the efficiency

of the coupling of the monochromatic wave into the optical fiber as the diffraction angle varies, similar to the situation above.

C. Readout of a SH ensemble using an optical frequency comb

A parallel readout of the ensemble of SHs is implemented by driving the AOM2 with the same rf comb signal that was used for burning the hole pattern. That is, the interrogating laser is now a frequency comb. Additionally, we periodically ($f_{\text{scan}} = 10$ Hz) sweep the whole comb over a small optical frequency interval of 100 kHz.

Figure 6 (top) shows the crystal transmission signal for interrogation by the optical comb. In this measurement the total laser power in front of the crystal was approximately $1 \mu\text{W}$, or about 2 nW per component. Each spectral feature may be called a compound spectral hole (CSH). When the mean frequency of the comb is appropriately set, i.e., centered on the SH ensemble, the CSH arises from all 512 previously burned SHs. With increasing absolute detuning, the subsequent CSHs arise from a decreasing number of SHs.

The S/N ratio of the CSHs is significantly improved compared to the one resulting from interrogating a single SH. To determine the improvement factor, single SHs were interrogated with the monochromatic laser, and with the power of the laser wave set to the same level as that of an individual component of the comb wave. The result is shown in Fig. 6

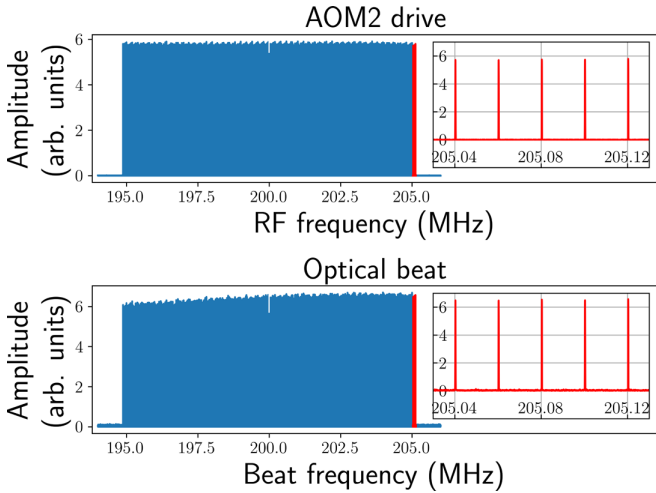


FIG. 4. Top: rf spectrum of the signal that drives AOM2, consisting of 512 components spaced by 20 kHz. Bottom: Optical spectrum of the heterodyne beat between the unmodulated laser wave f_L and the optical frequency comb. Note the dip in the center of the spectra, due to the partially suppressed rf carrier f_0 and the optical carrier $f_L + f_0$, respectively. Note also the missing two components $n = 1$ of the comb around the carrier f_0 as result of the characteristic of the DBM. Insets (red): the five highest-frequency components.

bottom. The laser was swept over the same frequency range as before. Note that the SHs were not burnt anew, but are from the same ensemble that has been used as in Fig. 6 (top). We find an approximately 20-fold improvement in the S/N ratio in the frequency-comb spectroscopy of the ensemble (top) compared to the spectroscopy of a single SH by a monochromatic laser wave (bottom). This value is approximately the expected

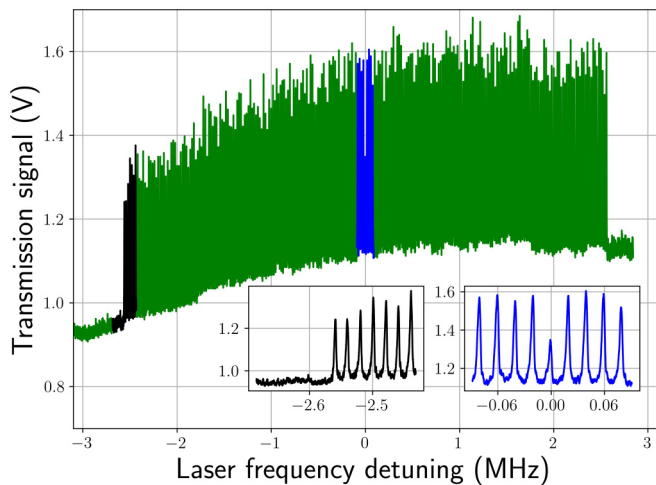


FIG. 5. Crystal transmission spectrum of an ensemble of 256 + 1 spectral holes, probed by a single-frequency laser (power approximately $1 \mu\text{W}$). The SHs were previously simultaneously burnt by an optical comb. The left inset shows enlarged several SHs located on the low-frequency end of the spectrum, marked in black. The right inset shows the center region of the ensemble with the smallest SH in the center burnt by the only partially suppressed optical carrier frequency $f_L + f_0$. Note that the components $n = 1$ are not filtered out as in Fig. 4 due to the use of a different DBM.

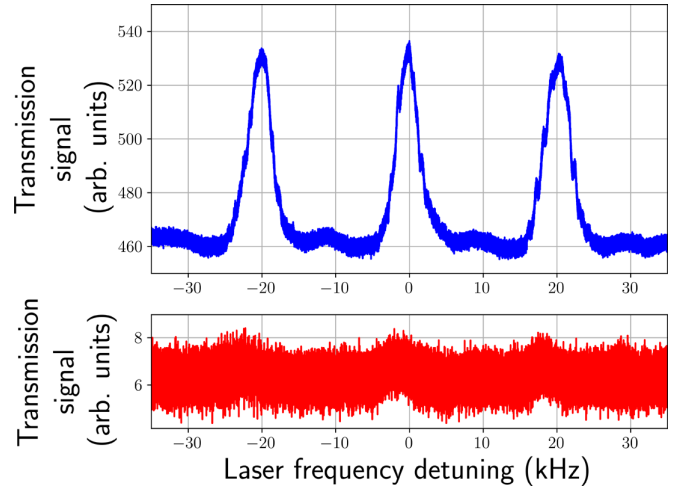


FIG. 6. Top: Compound spectral holes (CSHs) obtained from simultaneous interrogation of approximately 512 SHs by a laser frequency comb containing 512 spectral components. All components of the comb are tuned by the same amount during the scan. More precisely, the left CSH and the right CSH result from 511 SHs, while the central one results from 512 components. Bottom: Three SHs from the previous ensemble interrogated sequentially by a single-frequency laser. The laser wave power was set equal to the power of a single component of the comb in the top case. Note that the signal scales in the top and bottom plots are equal. The scan time was 100 ms. The detection bandwidth was 1 kHz. The two measurements have been taken approximately 2 h apart, resulting in a frequency shift that has been removed to center-align both plots.

improvement in S/N ratio, which by a simple argument is the square root of the number $2N = 512$ of spectral holes.

IV. LASER FREQUENCY STABILIZATION TO A SH ENSEMBLE

A. Frequency metrology system

The measurement of the stabilized 580-nm laser frequency was carried out by sending the laser radiation at 1160 nm via an actively path-length-stabilized optical fiber to our frequency metrology laboratory. This is indicated in the top right of Fig. 3. In that laboratory, we operate a femtosecond frequency comb (FFC). The FFC is locked to a ULE-cavity-stabilized laser at 1064 nm having a linewidth of approximately 1 Hz. This procedure reduces dramatically the linewidth of all spectral components of the FFC. The frequency of each FFC spectral component j is then given by $f_{\text{FFC},j} = f_{\text{ceo}} + j f_r = c_j f_{1064} + d_j f_{\text{ceo}}$, where f_{ceo} is the carrier envelope frequency, f_r is the repetition rate, f_{1064} is the laser frequency, and c_j and d_j are known numerical coefficients that depend on the mode number j .

The 1160-nm spectroscopy laser radiation ($f_L/2$) produces a beat signal $f_b = f_L/2 - f_{\text{FFC},m}$ with the closest spectral component m of the FFC, having frequency $f_{\text{FFC},m}$. The beat is detected using a high-speed photodetector. A characterization of this beat allows us to determine upper limits for the linewidth and for the frequency instability of the 1160-nm spectroscopy laser (see below).

In order to be able to precisely determine the instability of the spectroscopy laser when locked to the SHs, the rf signal f_b is sent to the spectroscopy laboratory via a coaxial cable. There we use a second DDS (DDS2) and a mixer to cancel out the frequency modulated (FM) sidebands in the spectrum of DDS1, creating an output signal having a monochromatic frequency $f_a = f_{\text{DDS2}} - f_0$. We use $f_{\text{DDS2}} = 260$ MHz. This procedure is necessary when an error signal is generated, as described in the following section. Using a frequency divider, we then generate the signal $f_a/2$ followed by a rf mixer to produce the rf analysis frequency $f_d = f_b - f_a/2$.

When locked to the CSH, the laser frequency is $f_L = -f_0 + f_{\text{CSH}}$, where f_{CSH} is the mean optical frequency of the hole ensemble. The rf analysis frequency is then

$$\begin{aligned} f_d &= f_L/2 - (c_m f_{1064} + d_m f_{\text{ceo}}) - (f_{\text{DDS2}} - f_0)/2 \\ &= f_{\text{CSH}}/2 - (c_m f_{1064} + d_m f_{\text{ceo}}) - f_{\text{DDS2}}/2. \end{aligned} \quad (3)$$

The coefficient c_m is approximately 1 since the wavelengths 1064 and 1160 nm are close. The term $f_{\text{DDS2}}/2$ is a known stable frequency and the constant d_m can be determined in a standard way.

Finally, the absolute frequency of the CSH is obtained by solving Eq. (3) for f_{CSH} . The absolute value of the 1064-nm laser frequency f_{1064} is needed to compute it and it is therefore measured with respect to an in-house hydrogen maser using the FFC.

B. Error signal generation

For laser frequency stabilization an error signal is necessary. For this purpose, the frequency comb as a whole can additionally be frequency modulated. We implement this by applying a modulation signal (modulation frequency $f_{\text{fm}} = 2.91$ kHz) to the summing amplifier driving the FM input of the DDS1 (Fig. 3). We characterize the frequency-modulated comb using the optical heterodyne beat measurement. A few components of the spectrum are shown in Fig. 7. We recognize the frequency modulation sidebands on each component of the comb.

For characterization of the error signal, the entire spectrum is furthermore additionally slowly frequency modulated via a triangular waveform at the scan frequency $f_{\text{scan}} \simeq 10$ Hz. The scan and the frequency modulation are added in a summing amplifier.

An ensemble of 1024 previously burnt SHs was interrogated with the frequency-modulated comb. The laser power in an individual spectral component was approximately 0.15 nW. The green trace in Fig. 8 (top) shows the laser power transmitted through the crystal while the laser frequency was slowly scanned. The effect of the imposed frequency modulation is clearly visible, because it leads to a modulation of the power transmitted through the crystal. The black line is the average of 170 successive scans of the CSH.

We used a lock-in amplifier (LIA) to demodulate the photodetector signal at 2.91 kHz. The demodulated signal at the output of the lock-in amplifier is shown in the bottom panel of the figure as an orange line. This represents a CSH error signal. The black line shows an average of repeatedly recorded error signals.

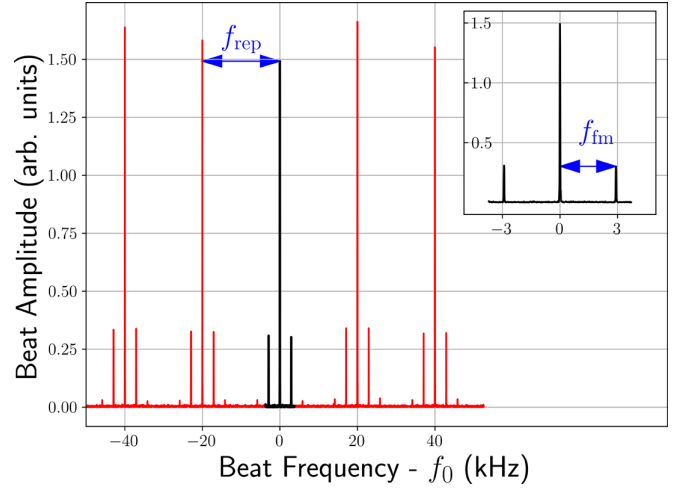


FIG. 7. A subset of spectral components of the optical frequency comb having an additional frequency modulation at a frequency $f_{\text{fm}} = 2.91$ kHz. This signal was recorded with the heterodyne optical beat at PD B. The inset shows one comb component and its modulation sidebands.

C. Frequency locking to a compound spectral hole

The comb spectroscopy radiation was locked to the ensemble of 1024 SHs by feeding back the error signal obtained at the output of the LIA to the FM input of DDS1 driving AOM2. Thereby, f_0 was continuously adjusted. The locking bandwidth was approximately 1 kHz, limited by the employed modulation frequency (2.91 kHz). Figure 9 (top) shows the result of a stabilization of the comb laser radiation to an ensemble of SHs by the frequency-comb technique. It

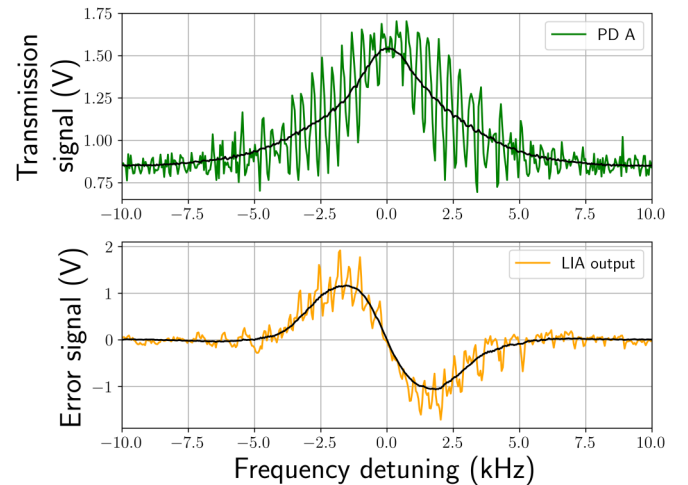


FIG. 8. Spectroscopy of a 1024-spectral hole ensemble performed by a frequency-modulated optical comb. Top: Raw signal (green) from the photodetector PD A as the comb is scanned over the spectral hole ensemble. This is a CSH. The (black) trace shows the average of 170 scans. Bottom: The output (orange) from a lock-in amplifier that detected the amplitude modulation of the transmitted power and converted it to a low-frequency signal. The black line shows the average of 170 scans. The scan range was 20 kHz and the scan period was 100 ms.

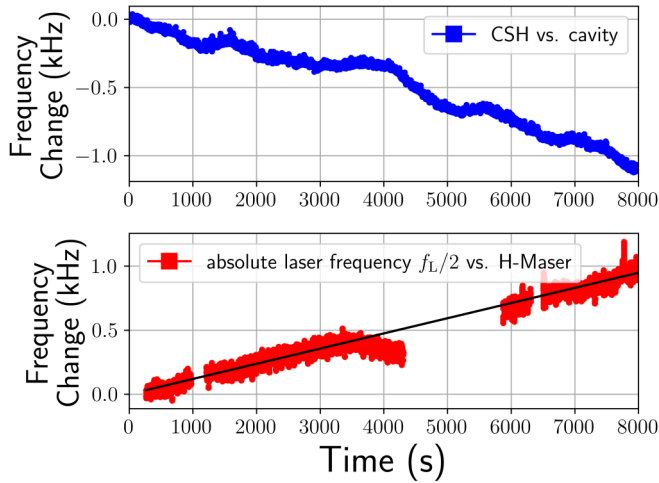


FIG. 9. Frequency stabilization by the CSH technique: A Schroeder-comb modulated 580-nm spectroscopy wave is locked to a previously burnt hole ensemble. Blue: Time trace of the AOM2 frequency f_0 that controls the offset of the mean frequency of the comb, $f_L + f_0$, relative to the ULE reference cavity (frequency f_L). The temperature of the crystal was approximately 5.8 K, and was actively stabilized. Bottom: Variation of the absolute frequency $f_L/2$ of the 1160-nm diode laser locked to its cavity, measured using a FFC and a hydrogen maser. The gap in the red time trace is due to a temporary malfunction of the FFC.

demonstrates a continuous locked operation for more than 2 h. The blue line shows the time trace of the variation of the AOM2 frequency f_0 , the frequency offset between the ULE cavity frequency and the mean frequency of the optical comb stabilized to the SH ensemble. Thus, a drift of f_0 reflects the combined drifts of the reference cavity and of the spectral hole ensemble. No significant degradation of the CSH error signal occurred. We checked this by scanning the error signal after stopping the frequency lock.

For comparison, the red trace in Fig. 9 shows the time variation of the absolute optical frequency $f_L/2$ of the diode laser stabilized to its ULE cavity. It was calculated from the recorded beat frequency f_b and from the simultaneously recorded values of the 1064-nm laser absolute frequency f_{1064} measured with the FFC. The observed drift rate amounts to approximately 51 mHz/s and is due to the cavity drift. The drift of the second harmonic f_L is thus approximately 100 mHz/s. It is twice as large in magnitude as the drift rate of f_0 , and has the opposite sign. We conclude that there is a net drift rate of approximately 50 mHz/s of the absolute mean frequency $f_L + f_0$ of the wave stabilized to the SH ensemble. We believe that this drift could be due to a residual burning effect by the interrogating comb [20].

For the frequency stability measurements, the crystal temperature was actively stabilized, with a residual instability at the level of 1 mK. This suppressed temperature-induced frequency variations of the SH frequencies to a sufficiently low level [27].

To determine the achievable stability on short time scales we used a CSH having 256 components at a temperature of about 4 K.

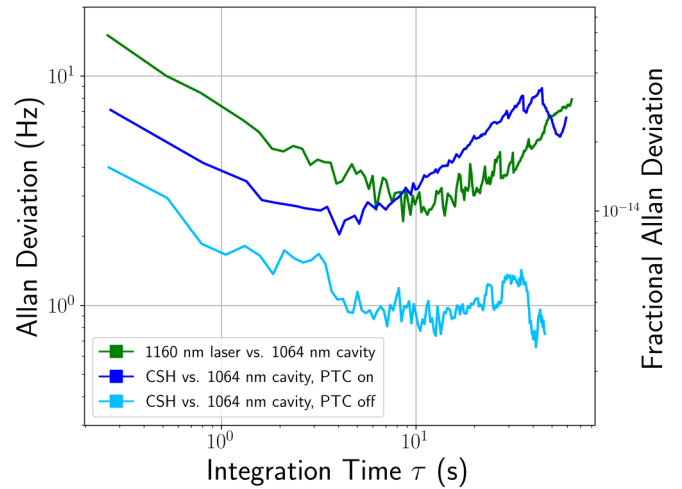


FIG. 10. Frequency stability of a laser locked to a compound spectral hole using comb spectroscopy. Blue: Allan deviation of the 1160-nm laser, $f_L/2$, when stabilized to the SH ensemble via comb spectroscopy, relative to the optically stabilized FFC, i.e., relative to the 1064-nm ULE cavity frequency. Here, the pulse tube cooler on the cryostat is on and the cryostat is in normal operation. Light blue: The pulse tube cooler is turned off. This trace is computed after the frequency drift due to crystal temperature rise was subtracted. The green trace shows a baseline performance: Allan deviation of the frequency difference of the cavity-stabilized 1160-nm laser and optically stabilized FFC, each stabilized to its respective ULE cavity.

First, to determine the performance level of the lasers and the metrology system, we measured the difference in optical frequencies between the 1160-nm laser stabilized to its cavity and the cavity-stabilized 1064-nm laser, via the FFC. For this purpose, we analyze the fluctuations of the beat frequency f_b , shown in green in Fig. 10. Strictly speaking, we thereby analyzed the variations of f_L with respect to the frequency $c_m f_{1064}$ according to Eq. (3). At 1-s integration time, the instability is at the level of 1×10^{-14} . The upturn of this trace for integration times beyond 10 s reflects the drifts of the two reference cavities.

The blue trace shows the frequency stability of the 1160-nm spectroscopy frequency when locked to the SH ensemble via comb spectroscopy, again relative to the frequency $c_m f_{1064}$. The relevant frequency analyzed was f_d . The upturn of its Allan deviation beyond 50-s integration time reflects the drifts of both the CSH reference and the 1064-nm reference cavity. The fact that the blue trace lies below the green trace for short integration times demonstrates the efficiency of the frequency lock to the SH ensemble.

One of the factors influencing the frequency stability of the SHs is the mechanical vibrations in the PTC cryostat. Mechanical strain applied to the $\text{Eu}^{3+} : \text{Y}_2\text{SiO}_5$ crystal deforms the lattice and thus shifts the energy levels of the dopants and, as a result, the frequency of a burnt SH [15,28]. In order to eliminate the effect of cryostat vibrations on SH stability, the cryostat was turned off for several minutes, and data were taken. This also led to a rapid increase of the temperature of the $\text{Eu}^{3+} : \text{Y}_2\text{SiO}_5$ crystal of a few hundred mK and, as a consequence, to a frequency drift of the SHs of approximately 2 kHz within 2 min. This temperature-induced shift is

consistent with the previously measured temperature dependence of 108 Hz/K^4 [27]. This linear drift was removed in the data analysis by subtracting a linear fit to the data. The result is the light blue curve in Fig. 10. The instability lies below the blue and the green curves, showing that indeed the instability is affected by the vibrations. The instability was thus reduced to a fractional level of 4×10^{-15} . Note that the reference for this measurement is the 1064-nm laser stabilized to its reference cavity. Thus, the minimum level reached by the light blue trace may contain a significant contribution from the instability of the 1064-nm laser, which from previous measurements we know to be of the same order [29].

V. DISCUSSION

We introduced a method for the spectroscopy of inhomogeneously broadened spectral lines and applied it to rare-earth-doped crystals. We modulated a laser wave into a comb of closely spaced spectral components and used it to burn, read out, and frequency lock to persistent spectral holes in a $\text{Eu}^{3+} : \text{Y}_2\text{SiO}_5$ crystal.

Our measurements showed that the power contained in a monochromatic input laser wave can be split rather evenly into up to 1000 spectral components, by use of a single acousto-optic modulator. In comparison to the work of Duran *et al.* [25] we achieve an almost flat comb spectrum.

Persistent spectral hole burning with such a comb resulted in a spectral hole ensemble containing up to 1000 individual spectral holes of similar depth. It is possible to read out in parallel the SH ensemble and this results in a compound

spectral hole (CSH). It appears less susceptible to spectral deformation by the inherent burning effect during interrogation and thus appears attractive as a frequency discriminator for frequency stabilization of lasers. The CSH also has a significantly improved S/N ratio compared to a single spectral hole. We demonstrated a frequency lock of a laser to a CSH and determined its frequency stability.

In contrast to the methods reported in Refs. [16–18] our method does not require any frequency-relocking techniques and delivers by design a continuously available error signal with a bandwidth of approximately 1 kHz. The introduced method is a step towards increasing the stability of frequency locks based on spectral holes as it greatly improves the signal strength of the frequency discriminator while being able to reduce the alterations of the *individual* SH.

One important future activity is to study the origin of the drift observed in the frequency locking demonstration, for example, by varying the number of spectral holes, the laser power, or the crystal temperature.

Finally, it appears possible to apply variations of the present frequency-comb technique to other systems exhibiting inhomogeneous spectral broadening.

ACKNOWLEDGMENTS

The authors thank D. Iwaschko for his skilled technical assistance and Michael G. Hansen, E. Wiens, and I. Kortunov for contributing to the optical frequency measurements. This work was partially performed in the framework of Project No. Schi 431/15-1 of the Deutsche Forschungsgemeinschaft.

-
- [1] W. R. Milner, J. M. Robinson, C. J. Kennedy, T. Bothwell, D. Kedar, D. G. Matei, T. Legero, U. Sterr, F. Riehle, H. Leopardi, T. M. Fortier, J. A. Sherman, J. Levine, J. Yao, J. Ye, and E. Oelker, *Phys. Rev. Lett.* **123**, 173201 (2019).
 - [2] E. Oelker, R. B. Hutson, C. J. Kennedy, L. Sonderhouse, T. Bothwell, A. Goban, D. Kedar, C. Sanner, J. M. Robinson, G. E. Marti *et al.*, *Nat. Photonics* **13**, 714 (2019).
 - [3] N. Huntemann, C. Sanner, B. Lipphardt, C. Tamm, and E. Peik, *Phys. Rev. Lett.* **116**, 063001 (2016).
 - [4] S. M. Brewer, J.-S. Chen, A. M. Hankin, E. R. Clements, C. W. Chou, D. J. Wineland, D. B. Hume, and D. R. Leibbrandt, *Phys. Rev. Lett.* **123**, 033201 (2019).
 - [5] I. Ushijima, M. Takamoto, M. Das, T. Ohkubo, and H. Katori, *Nat. Photonics* **9**, 185 (2015).
 - [6] D. G. Matei, T. Legero, S. Häfner, C. Grebing, R. Weyrich, W. Zhang, L. Sonderhouse, J. M. Robinson, J. Ye, F. Riehle, and U. Sterr, *Phys. Rev. Lett.* **118**, 263202 (2017).
 - [7] J. M. Robinson, E. Oelker, W. R. Milner, W. Zhang, T. Legero, D. G. Matei, F. Riehle, U. Sterr, and J. Ye, *Optica* **6**, 240 (2019).
 - [8] T. Kessler, C. Hagemann, C. Grebing, T. Legero, U. Sterr, F. Riehle, M. J. Martin, L. Chen, and J. Ye, *Nat. Photonics* **6**, 687 (2012).
 - [9] M. Notcutt, L.-S. Ma, A. D. Ludlow, S. M. Foreman, J. Ye, and J. L. Hall, *Phys. Rev. A* **73**, 031804(R) (2006).
 - [10] R. M. MacFarlane and R. M. Shelby, *Coherent Transient and Holeburning Spectroscopy of Rare Earth Ions in Solids*, Modern Problems in Condensed Matter Sciences Vol. 21 (Elsevier, Amsterdam, 1987), Chap. 3, pp. 51–184.
 - [11] G. J. Pryde, T. Böttger, R. L. Cone, and R. C. C. Ward, *J. Lumin.* **98**, 309 (2002).
 - [12] T. Böttger, G. J. Pryde, and R. L. Cone, *Opt. Lett.* **28**, 200 (2003).
 - [13] P. B. Sellin, N. M. Strickland, J. L. Carlsten, and R. L. Cone, *Opt. Lett.* **24**, 1038 (1999).
 - [14] M. J. Sellars, R. S. Meltzer, P. T. H. Fisk, and N. B. Manson, *J. Opt. Soc. Am. B* **11**, 1468 (1994).
 - [15] M. J. Thorpe, L. Rippe, T. M. Fortier, M. S. Kirchner, and T. Rosenband, *Nat. Photonics* **5**, 688 (2011).
 - [16] D. R. Leibbrandt, M. J. Thorpe, C.-W. Chou, T. M. Fortier, S. A. Diddams, and T. Rosenband, *Phys. Rev. Lett.* **111**, 237402 (2013).
 - [17] S. Cook, T. Rosenband, and D. R. Leibbrandt, *Phys. Rev. Lett.* **114**, 253902 (2015).
 - [18] O. Gobron, K. Jung, N. Galland, K. Predehl, R. L. Targat, A. Ferrier, P. Goldner, S. Seidelin, and Y. L. Coq, *Opt. Express* **25**, 15539 (2017).
 - [19] N. Galland, N. Lučić, S. Zhang, H. Alvarez-Martinez, R. L. Targat, A. Ferrier, P. Goldner, B. Fang, S. Seidelin, and Y. L. Coq, *Opt. Lett.* **45**, 1930 (2020).
 - [20] B. Julsgaard, A. Walther, S. Kröll, and L. Rippe, *Opt. Express* **15**, 11444 (2007).

- [21] R. Yano, M. Mitsunaga, and N. Uesugi, *Phys. Rev. B* **45**, 12752 (1992).
- [22] Y. S. Bai and M. D. Fayer, *Phys. Rev. B* **39**, 11066 (1989).
- [23] T. Sakamoto, T. Kawanishi, and M. Izutsu, *Electron. Lett.* **43**, 1039 (2007).
- [24] Q. Wang, L. Huo, Y. Xing, and B. Zhou, *Opt. Lett.* **39**, 3050 (2014).
- [25] V. Duran, C. Schnebelin, and H. G. de Chatellus, *Opt. Express* **26**, 13800 (2018).
- [26] M. Schroeder, *IEEE Trans. Inf. Theory* **16**, 85 (1970).
- [27] R. Oswald, M. G. Hansen, E. Wiens, A. Y. Nevsky, and S. Schiller, *Phys. Rev. A* **98**, 062516 (2018).
- [28] N. Galland, N. Lučić, B. Fang, S. Zhang, R. Le Targat, A. Ferrier, P. Goldner, S. Seidelin, and Y. Le Coq, *Phys. Rev. Appl.* **13**, 044022 (2020).
- [29] Q.-F. Chen, A. Nevsky, M. Cardace, S. Schiller, T. Legero, S. Häfner, A. Uhde, and U. Sterr, *Rev. Sci. Instrum.* **85**, 113107 (2014).